Supplementary Materials

David Reens,* Hao Wu,* Tim Langen,† and Jun Ye
JILA, National Institute of Standards and Technology and the University of Colorado and Department of Physics, University of Colorado, Boulder, Colorado 80309-0440, USA
(Dated: September 19, 2017)

The present study on the role of mixed fields for spin-flip loss evolved out of our continuing investigations into the collisional processes reported in Refs. [1, 2]. These investigations have revealed that an important fraction of the effects attributed to collisions are in fact attributable to spin-flip losses. In Sec. A and Sec. B we provide the interested reader with our current best understanding of the situation. Lastly, we provide in Sec. C an algebraic derivation of the loss enhancement factor presented in Eqn. 3 of the main text [3].

A. Electric Field Induced Collisions

We begin with Ref. [1] on electric field induced inelastic collisions. The authors identified the same single particle spin-flip loss enhancement process we discuss [3], and an attempt was made at deconvolution from the collisional effect (App. A, Ref. [1]). Since that time, new observations prompted us to make an even more careful investigation, during which we discovered an important mathematical improvement.

Relative to the approach taken in App. A of Ref. [1], we make the same simplifying assumptions: loss only occurs in the $\vec{E} \perp \vec{B}$ plane, only the velocity orthogonal to this plane matters, and the population is a thermalized Maxwell-Boltzmann distribution. Our correction relates to the next step, where an integral calculation for the loss rate is performed. In Ref. [1] the integration spans the entire 3D spatial distribution, weighted by the frequency of crossing of the center plane and the chance of loss for each crossing:

$$\Gamma_{\mathrm{LZ}} = \int_0^\infty 4\pi r^2\, n(r) dr \int_0^\infty n(v_\theta) dv_\theta \left(\frac{v_\theta}{\pi r} P_{\mathrm{hop}}(r, v_\theta)\right) \quad (1)$$

Here $n(r)$ is the radial distribution function, constrained to satisfy $\int_0^\infty 4\pi r^2 n(r) = 1$, and of the form $n(r) \propto e^{-\mu_B B`r/kT}$. Likewise $n(v_\theta)$ is the usual normalized Maxwellian velocity distribution. Implicit in this integration is the assumption that molecules at a given radius r cross the center plane with a frequency of $v_\theta/\pi r$. This approximation is rather rough given that molecules are certainly not following circular orbits of constant v_θ but are in general following some complex trap motion. Our correction is to perform an integration of flux through the loss plane directly:

$$\Gamma_{\mathrm{LZ}} = \int_0^\infty 2\pi r\, n(r) dr \int_0^\infty n(v_z) dv_z \left(v_z P_{\mathrm{hop}}(r, v_z)\right) \quad (2)$$

Here the same distributions are used, but the spatial is integrated over the central plane only, hence the $2\pi r$ Jacobean, and the hopping probability is multiplied by v_z to give a flux. The coordinates z and θ are mathematically equivalent in the central plane. This flux integral gives the desired loss rate without any approximations about molecule orbits or plane-crossing frequency. Although the two integrals differ significantly in conception, mathematically the differences reduce to precisely an overall scaling factor of π.

The influence of this on the deconvolution procedure relates to the details of the two-body fitting routine. One plus two body fits $\dot{N} = -\gamma N - \beta N^2$ were performed to various decay trap curves, with the one body rate γ fixed to the value expected due to vacuum scattering and spin-flip loss. An example of such decay curves is shown in Fig. S1, where electric field is turned on suddenly after various hold times. With the stronger spin-flip loss, it is no longer appropriate to assume this loss will be present in the data as a pure one-body decay. Rather, only those molecules whose orbits regularly intersect the loss region are lost, after which thermalization would be required to repopulate the loss prone trajectories of phase space. If

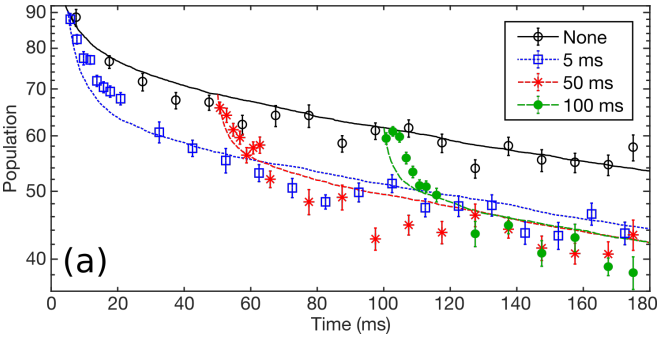

FIG. S1. Experimental electric field induced loss data with an attempted overlap to spin-flip loss simulations. The case of no electric field (black, solid) is compared to electric fields of 3 kV/cm turned on after a wait time indicated in the legend.

* Contributed equally. Email dave.reens@colorado.edu or hao.wu@colorado.edu.
† Present Address: 5. Physikalisches Institut and Center for Integrated Quantum Science and Technology (IQST), Universität Stuttgart, Pfaffenwaldring 57, 70569 Stuttgart, Germany

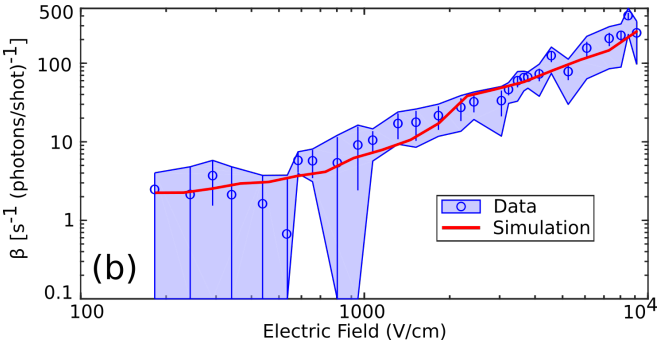

FIG. S2. Two body fits from [1] to experimental data like that in Fig. S1 but at various electric fields. The blue data points and shaded region are repeated from Fig. 3 of [1], where the shading indicates the variation that would be brought about by changes in the single particle effect by a factor of two in either direction. Even though we discover a factor of only three, the spin flip loss simulation (thick red solid line) matches the data within errorbars.

thermalization is slow, spin-flip loss can have a rate that decreases over time, producing a time dependence of population like that of a two-body effect. Even though the possibility of a factor of two error in the calculated magnitude of spin-flip loss was considered in Ref. [1] (Fig. S2, shaded regions), the possibility of its influencing the data in a non-single-particle manner was not addressed.

We can perform single particle simulations of spin-flip loss to investigate this, and we obtain curves such as shown above the time dependent experiment data points in Fig. S1. We can even perform the same one plus two body fitting procedure to the single particle spin-flip loss simulation traces. The single particle traces yield "two-body" values that overlap nicely with those derived in Ref. [1], see Fig. S2. This suggests that the effect attributed to two-body collisions is largely explained by spin-flip losses. Still, there are notable differences, such as in the initial rate of the decays in Fig. S1. One avenue to try and improve agreement would be to incorporate collisions in the simulation. Unfortunately there are many challenges in the quantitative application of these simulations, such as the existence of various partially trapped substates. We think the best path forward is to perform future collisional studies with the single-particle effect removed, as achieved in our most recent trap [3].

B. Evaporation

With regard to Ref. [2], the present study has important ramifications. The process of evaporation and of depletion spectroscopy both require two steps. First molecules are transferred from positive to negative parity by microwaves targeting a specific range of magnetic fields. After this transfer, the molecules are still trapped, and only by the subsequent addition of electric field to open avoided crossings can these opposite parity molecules escape from the trap. In the case of depletion spectroscopy, there is a final step of measuring the population by laser induced fluorescence, so that the population originally at the magnetic field transferred by microwaves can be inferred by subtraction. The crossings opened by electric field would only allow molecules in the upper 90% of the trap to escape, so it was thought that a cold population insensitive to the spectroscopic technique could be building up at low magnetic fields. Given the existence of spin-flip loss caused by the electric field at the very center of the trap where such a cold population would build up, we reject this hypothesis. Since it was essential to the temperature fits performed in Fig. 3 of Ref. [2], they are therefore no longer trustworthy.

Nonetheless, without fitting temperatures, it is still possible to use normalized spectra to look for enhancements in density caused by the evaporation. We repeatably find such enhancements for evaporation sequences designed to achieve a twofold temperature reduction, see Fig. S3. The initial temperature of 59 ± 2 mK is higher than reported in Ref. [2] due to an important correction to the molecular Hamiltonian found by inclusion of nearly one hundred total ground and excited hyperfine levels [4].

Regarding the normalization procedure, the idea is to require the area beneath the curve to add up to the observed total population by laser induced fluorescence. An important question however is why this is necessary. The spectroscopy is performed by depleting molecules from a given region of the trap over a total time of about a quarter of a trap oscillation, so that molecules are not at all frozen in place. Relative to a very brief spectroscopy pulse that would only deplete molecules in a given region at that particular instant, the longer pulse can be seen as a way of boosting the signal to noise ratio of the experiment. The spectroscopy still gives a value that ought to be proportional to the true instantaneous population in the region of interest, but with a scaling factor relating to details of population transfer in and out of the region of interest while it is probed. Without normalization, spectroscopies of smaller total populations yield distributions with enclosed areas that are decreased much more than the actual population. In the future, a variety of density enhancing strategies [3] may improve our signal enough that a more straightforward spectroscopy could be performed without the need for normalization. For the time being, we find no particular reason to distrust the normalization procedure, and we carefully include all of the steps in the error analysis leading to the traces shown in Fig. S3.

Seeking to more thoroughly corroborate this observation in a way that does not depend on normalizations, we have compared the populations under two related conditions- the first a normal evaporation sequence and the second an evaporation with time-reversed microwave frequency, so that the cut goes backwards from deep to shallow. We refer to these conditions as forward and

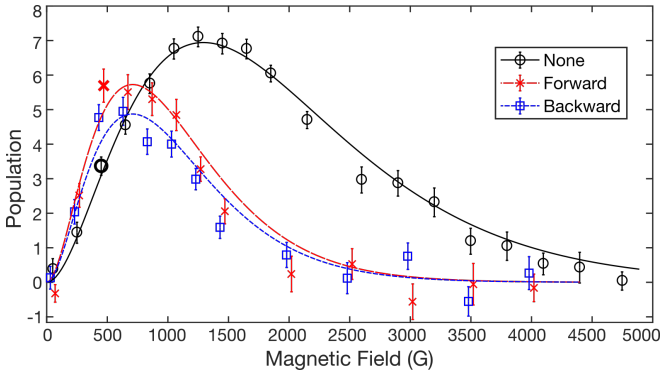

FIG. S3. Normalized spectra are performed under three conditions: one with no evaporation (black circles), one with an exponential RF evaporation ramp over 170 ms (red x's), and a third with this ramp applied in a time reversed manner (blue squares). Solid lines are fits to Maxwell-Boltzmann distributions with temperatures of 59 ± 2 in the case of no evaporation (black), and 30 ± 3 for both forward (red, long dashes) and backward (blue, short dashes) evaporations. The forward evaporation achieves a clear density enhancement in the vicinity of 500 G, where the line markers are bolded.

backward evaporation, respectively. This comparison subjects all molecules to the same integrated microwave power, and thus the two conditions should be equivalent in a situation with only single particle effects. However, with respect to collisional effects, the time-reversed case functions like a truncation, preventing molecules that would otherwise have collisionally thermalized to lower temperatures from doing so. To whatever extent an evaporation is successful in facilitating beneficial thermalizing collisions, the time-reversed condition should yield fewer molecules. We consistently observe this, at about the 5% level, note the height difference in the traces shown in Fig. S3. One puzzle however is that the observed spectra are only different by a scaling factor; both fit to 30 ± 3 mK. One might have expected the forward evaporation to yield more molecules at lower fields relative to the backward and thus fit a colder temperature. It could be that the collisional effect is strong enough to show an effect in final molecule number, but that more collisions are required before the spectra are distinguishable in shape and temperature. It is also possible that the forward evaporation would show a clearer shift in the distribution if not for competition with the influence of spin-flip losses at the trap center.

More recently, we have developed the ability to reduce population without perturbing phase space distribution, mentioned and used to look for collisions in our new trap as described in the main text [3]. This ought to reduce the influence of collisional processes, but keep any single particle effects the same, thus disambiguating the two. Many possible approaches have key drawbacks, for example changing the partial pressure of water in our supersonic expansion would require changing the temperature of the valve and thereby influencing the initial beam temperature. We opt for the application of microwaves during deceleration, leading to a probability for transitioning from a weak to strong field seeking state and being deflected out of the beam. We tune the microwaves to be resonant to such a transition at low magnitudes of electric fields, experienced by all molecules when flying through a de-energized stage just after switching. The microwaves are applied via microwave horn and have a long wavelength relative to the cloud, so that microwave power variations across the cloud are not relevant. The microwaves are applied early during deceleration, so that the molecules have many stages of deceleration left to remix any outstanding asymmetries in the removal process. It is difficult to experimentally verify that the phase space distribution is truly unaffected in all six dimensions, but in at least one projection of phase space, the time of flight profile of slowed molecules after deceleration, the distribution is unaffected even by tenfold reductions using this technique.

In conclusion, the role of collisional effects in Ref. [1] is reduced by spin-flip losses, but spectroscopic comparisons and evaporation subtractions still suggest an evaporative effect. The development of various sensitive tools has us poised to more unambiguously identify any future collisional effects in our next generation system.

C. Scaling Law Derivation

Here we derive the loss enhancement scaling law presented in Eqn. 3 of the main text [3], and repeated here:

$$\eta \propto \left(\frac{d_{\text{eff}} E}{\sqrt{\kappa \Delta}}\right)^{8/3}. \tag{3}$$

The key idea is to compare the surface areas of the loss regions with and without electric field. There is no exact loss region where a molecule is guaranteed to hop, but rather its velocity and direction contribute to the Landau-Zener probability (Eqn. 2, Ref. [3]). Nonetheless, for the purposes of a scaling law, we can assume the average thermal velocity v_T, and choose a probability threshold of $P > 1/e$. These assumptions allow us to define the loss region as the contour surface of energy κ where

$$\kappa = \sqrt{\hbar \dot{G}} = \sqrt{2\hbar v_T B'}; \tag{4}$$

G is the energy gap between the trapped state and its spin flip partner, and B' is the trap gradient.

One complication is that in a quadrupole trap there is a weak and a strong axis. We assume that the electric field is applied parallel to the strong axis, which makes the loss plane where $\vec{E} \perp \vec{B}$ perpendicular to the strong axis. This matches the geometry that has been realized in our experiment [1], and is the worst case, but by no more than a constant factor of $2\sqrt{2}$ relative to other directions the electric field could have. We always use B' to refer to the stronger gradient.

Before application of electric field, the κ valued energy contour is an oblate ellipsoid of long radius $r_0 = 2\kappa/\mu_{\rm eff}B'$. Its area is then $2\pi \cdot 1.38 r_0^2$, where the prefactor comes from the specific $2:1$ aspect ratio of the ellipsoid and is hereafter neglected. When electric field is applied, the energy gap near the trap zero takes the following functional form:

$$G = \mu_{\rm eff}B'|z| + \alpha(\frac{1}{2}\mu_{\rm eff}B'r)^3\frac{\Delta\sqrt{\beta\Delta^2+d_{\rm eff}^2E^2}}{(d_{\rm eff}E)^4}, \quad (5)$$

plus higher order terms in r and z. Here we use r to denote the in-loss-plane coordinate and z to denote distance away from the loss plane, along the strong axis of the trap. The constants α and β are nearly unity for OH and will be ignored henceforth. This is a series expansion the energy difference between the trapped state and its spin-flip-partner. The energy difference can be derived for OH by diagonalizing the ground state hamiltonian in mixed fields, see App. A of Ref. [5], or similarly for any other species.

Now we use Eqn. 5 to compute the area of the surface $G = \kappa$. We specialize to the regime where $d_{\rm eff}E < \Delta$, so that $\Delta \approx \sqrt{\Delta^2 + d_{\rm eff}^2E^2}$. For larger fields, one Δ can be exchanged for $d_{\rm eff}E$, but in practice the loss rate is already so high in these regimes that no sample remains trapped. The radial extent of the surface can be solved by inverting $\kappa = G|_{z=0}$:

$$r_E = \frac{1}{\mu_{\rm eff}B'}\sqrt[3]{\frac{8\kappa(d_{\rm eff}E)^4}{\Delta^2}}. \quad (6)$$

The axial extent remains $z = \kappa/\mu_{\rm eff}B'$ for all $\vec{E}$. For large enough E, r_E dominates over this axial extent, so that the area is effectively $2\pi r_E^2$ and the loss area enhancement becomes $\eta = (r_E/r_0)^2$. Comparing the expressions for r_E and r_0, $\mu_{\rm eff}B'$ cancels and we have

$$\eta = \left(\frac{1}{2\kappa}\sqrt[3]{\frac{8\kappa(d_{\rm eff}E)^4}{\Delta^2}}\right)^2 = \left(\frac{d_{\rm eff}E}{\sqrt{\kappa\Delta}}\right)^{8/3}. \quad (7)$$

Now we address the domain of validity of this result. When E is small, Eqn. 5 only has a narrow range of validity, since the electric field only dominates in a very small region near the trap center. Outside, G retains a nearly linear dependence on r. This means that Eqn. 6 only holds for E above some threshold. For smaller E, r_E will simply not be significantly perturbed from its zero electric field value of $r_0 = 2\kappa/\mu_{\rm eff}B'$. The implication for the enhancement factor in Eqn. 7 is simply that it is only valid when it predicts an enhancement significantly greater than unity. In other words, Eqn. 7 holds when $d_{\rm eff}E > \sqrt{\kappa\Delta}$, but below this η gradually returns to unity. Eventually when $d_{\rm eff}E > \Delta$, the factor of $\sqrt{\beta\Delta^2 + d_{\rm eff}^2E^2}$ in Eqn. 5 is better approximated by $d_{\rm eff}E$, which leads to the modification $\eta \propto (d_{\rm eff}E)^2/\kappa^{4/3}\Delta^{2/3}$. Thus for these larger E-fields, the enhancement factor reduces in its dependence on electric field from order 8/3 to order 2. At this point, the loss is typically so large as to preclude all but the briefest trapping experiments, see Tab. I of the main text [3].

[1] B. K. Stuhl, M. Yeo, M. T. Hummon, and J. Ye, Molecular Physics **111**, 1798 (2013).
[2] B. K. Stuhl, M. T. Hummon, M. Yeo, G. Quéméner, J. L. Bohn, and J. Ye, Nature **492**, 396 (2012).
[3] See Main Text.
[4] K. Maeda, M. L. Wall, and L. D. Carr, New Journal of Physics **17**, 45014 (2015).
[5] B. K. Stuhl, M. Yeo, B. C. Sawyer, M. T. Hummon, and J. Ye, Physical Review A **85**, 033427 (2012).